Th-substituted SmFeAsO: Structural details and superconductivity with T_c above 50 K

N. D. Zhigadlo,[1,*] S. Katrych,[1] S. Weyeneth,[2] R. Puzniak,[2,3] P. J. W. Moll,[1] Z. Bukowski,[1] J. Karpinski,[1] H. Keller,[2] and B. Batlogg[1]

[1]*Laboratory for Solid State Physics, ETH Zurich, Schafmattstrasse 16, CH-8093 Zurich, Switzerland*

[2]*Physik-Institut der Universität Zürich, Winterhurerstrasse 190, CH-8057 Zürich, Switzerland*

[3]*Institute of Physics, Polish Academy of Sciences, Aleja Lotników 32/46, PL-02-668 Warsaw, Poland*

(Received 1 June 2010; revised manuscript received 9 July 2010; published 24 August 2010)

We report structural, magnetic, and transport properties of polycrystalline samples and single crystals of superconducting $Sm_{1-x}Th_xFeAsO$ with maximal T_c above 50 K, prepared under high pressure. Bulk superconducting samples do not undergo a structural phase transition from tetragonal to orthorhombic symmetry at low temperatures. The unit-cell parameters a and c shrink with Th substitution and the fractional atomic coordinate of the As site z_{As} remains almost unchanged while that of Sm/Th $z_{Sm/Th}$ increases. Upon warming from 5 to 295 K the increase in the FeAs layer thickness is dominant, while the changes in the other structural building blocks are minor, and they compensate each other, since the As-Sm/Th distance contracts by about the same amount as the O-Sm/Th expands. The polycrystalline and single-crystalline samples are characterized by a full diamagnetic response in low magnetic field, by a high intergrain critical current density for polycrystalline samples, and by a critical current density on the order of 8×10^5 A/cm^2 for single crystals at 2 K in fields up to 7 T. The magnetic penetration depth anisotropy γ_λ increases with decreasing temperature, in a similar way to that of $SmFeAsO_{1-x}F_y$ single crystals. The upper critical field estimated from resistance measurements is anisotropic with slopes of ~5.4 T/K ($H\|ab$ plane) and ~2.7 T/K ($H\|c$ axis), at temperatures sufficiently far below T_c. The low-temperature upper critical field anisotropy γ_H is in the range of ~2, consistent with the tendency of a decreasing γ_H with decreasing temperature, previously reported for $SmFeAsO_{1-x}F_y$ single crystals.

DOI: 10.1103/PhysRevB.82.064517 PACS number(s): 81.10.−h, 74.70.Dd, 74.62.Bf, 74.25.−q

I. INTRODUCTION

Renewed interest in the research of high-T_c superconductivity has been stimulated by the discovery of superconductivity in $LaFeAsO_{1-x}F_x$ ($T_c\sim26$ K),[1] followed by the substantial increase in T_c up to ~55 K (Refs. 2–4) by replacing La with other rare-earth elements (Ce, Pr, Nd, Sm, Gd, Tb, Dy, Ho, and Y).[2–10] In all members of the so-called 1111-*Ln*Fe*Pn*O family (*Ln*: lanthanide, *Pn*: pnictogen) the Fe_2Pn_2 layer is essential for superconductivity while the Ln_2O_2 layer plays a role of a charge-carrier source. A distinctive feature of this family is that the charge-carrier density and thus the electronic properties can be changed through chemical substitution at every atomic site. Electron doping can be realized by the partial substitutions of F for O (Ref. 6) as well as by oxygen deficiency.[11] In addition to the charge-carrier doping in Ln_2O_2 layers, the partial substitution of Fe with Co or Ni also leads to superconductivity.[12,13] Although the valence of Co and Ni ions seems to remain 2+, additional electrons are thought to be induced owing to the itinerant character of the 3*d* electrons.[12] Recent calculations of Wadati *et al.*[14] show that the extra *d* electrons are almost totally located within the muffin-tin sphere of the substituted site. It is suggested that Co and Ni act more like random scatterers, scrambling the momentum space and washing out parts of the Fermi surface. Apart from chemical doping, superconductivity develops when "chemical pressure" is generated by partial substitution of smaller and isovalent P ions for As in LaFeAsO.[15] Finally, *Ln* in the 1111-type structure can be also easily substituted. Superconductivity induced by doping with holes was reported in the case of Sr-substituted $Ln_{1-x}Sr_xFeAsO$ (*Ln*=La, Pr, and Nd),[16] while "electron-doped" superconductors were obtained through Th^{4+} substitution at the lanthanide site in GdFeAsO,[17] NdFeAsO,[18] and LaFeAsO (Ref. 19) with T_c's up to 56 K, 38 K, and 30 K, respectively. Superconductivity in Th and F codoped polycrystalline $Sm_{0.9}Th_{0.1}FeAsO_{1-y}F_y$ was reported too.[20] Thorium substitution, besides being carrier source, plays an important role in stabilization of the 1111 phase with smaller lanthanides such as Tb (see, for example, Ref. 21). Since the 1111 compounds still have the highest T_c among pnictides and are considered promising materials for future applications,[22] further investigations are desirable.

In this paper, we report the high-pressure synthesis and single-crystal growth of superconducting $Sm_{1-x}Th_xFeAsO$ in which the charge-carrier density is increased by substitution of Th^{4+} for Sm^{3+}. The studied materials exhibit bulk superconductivity with transition temperature above 50 K and with high critical current density.

II. EXPERIMENTAL DETAILS

Polycrystalline samples and single crystals of $Sm_{1-x}Th_xFeAsO$ were obtained in a cubic anvil high-pressure cell. Polycrystalline samples with nominal compositions of $Sm_{1-x}Th_xFeAsO$ (x=0, 0.08, 0.1, 0.15, 0.20, and 0.30) were prepared using SmAs, ThAs, Fe_2O_3, and Fe powders as starting materials. SmAs and ThAs were synthesized by reacting Sm turnings or Th foil with As pieces in evacuated and sealed silica ampoules at 850 °C for 3 days. Single crystals of Th-substituted SmFeAsO have been grown using $Sm_{0.7}Th_{0.3}FeAsO$ and $Sm_{0.65}Th_{0.35}FeAsO$ nominal composi-

tions and NaCl/KCl as a flux. The precursor to flux ratio was fixed to 1:1. The precursor powders were mixed and ground, and pressed into pellets in a glove box filled with dry argon gas. The growth conditions were similar to those applied for the growth of $SmFeAsO_{1-x}F_y$ single crystals.[23] Pellets containing precursor and flux were placed in a boron nitride crucible inside a pyrophyllite cube with a graphite heater. The six tungsten carbide anvils generated pressure on the whole assembly. In a typical crystal growth run, a pressure of 3 GPa was applied at room temperature. While keeping the pressure constant, the temperature was ramped up to 1430 °C within 1 h, maintained for 65 h, and decreased in 1 h to room temperature. For the synthesis of polycrystalline samples the maximum temperature was maintained for 4.5 h, followed by quenching. Then the pressure was released, the sample extracted and in the case of crystal growth NaCl/KCl flux was dissolved in water. Though conditions of crystal growth still require further optimization, we were able to grow plate-like single crystals with a size of $\sim 100 \times 100\ \mu m^2$.

Powder x-ray diffraction (XRD) investigations were performed at room temperature on a STOE diffractometer (Cu $K\alpha$ radiation) equipped with a mini-phase-sensitive detector and a Ge monochromator on the primary beam. Three powder samples with starting composition ($Sm_{1-x}Th_xFeAsO$, $x=0.08$, 0.15, and 0.3) were investigated at temperatures from ~5 to 295 K, using synchrotron radiation (Swiss-Norwegian beam lines at the European Synchrotron Radiation Facility, Grenoble, France) and a mar345 image-plate area detector (the sample to detector distance of 250 mm was calibrated using a Si standard, $\lambda=0.7000$ Å). The temperature was controlled with an accuracy of 1 K. The two-dimensional diffraction images were integrated using the program FIT2D (Ref. 24) and the one-dimensional powder patterns were refined with the FULLPROF program in a sequential mode.[25] Single-crystal structural investigations were done at room temperature using an x-ray single-crystal Xcalibur PX, *Oxford Diffraction* diffractometer equipped with a charge-coupled-device area detector, which allowed us to examine the whole reciprocal space (Ewald sphere). Data reduction and the analytical absorption correction employing indexing of crystal faces were introduced using the CRYSALIS software package.[26] The crystal structure was determined by a direct method and refined on F^2, employing the SHELXS-97 and SHELXL-97 programs.[27,28]

Magnetic measurements were performed in a *Quantum Design* magnetic property measurement system (MPMS XL) with the reciprocating sample option installed. The magnetic torque was measured using a highly sensitive miniaturized piezoresistive torque sensor within a home-made experimental setup described elsewhere.[29,30] This technique allows measurements of the angular-dependent superconducting magnetic behavior by detecting the torque of a single crystal in a magnetic field along a chosen orientation with respect to the crystallographic c axis. Four-point resistivity measurements were performed in a 14 T *Quantum Design* physical property measurement system (PPMS). Micrometer-sized Pt leads were precisely deposited onto a plate-like crystal using a focused ion beam method without altering the bulk superconducting properties.[22]

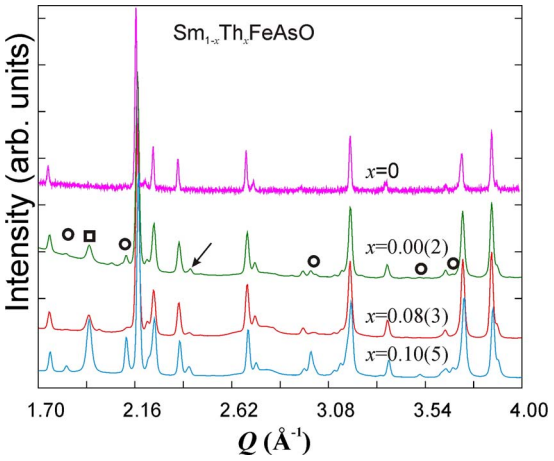

FIG. 1. (Color online) XRD patterns for polycrystalline samples of $Sm_{1-x}Th_xFeAsO$ [$x=0$, 0.00(2), 0.08(3), and 0.10(5); nominally: 0, 0.08, 0.15, and 0.3, respectively]. The values of x were determined by refining x-ray powder-diffraction data. The peaks marked by circles and square belong to SmAs and ThO_2, respectively. The arrow marks scattering from the sample container. $Q=4\pi \sin\theta/\lambda = 2\pi/d$. Note, in the sample with the smallest nominal Th content (nominally 0.08) it was impossible to refine it with reliable value (Table I).

III. RESULTS AND DISCUSSION

A. Crystal structure

Figure 1 depicts XRD patterns of the polycrystalline $Sm_{1-x}Th_xFeAsO$ samples with refined composition of $x=0.00$, 0.00(2), 0.08(3), and 0.10(5). The parent compound is essentially single phase and the main peaks of Th-substituted samples can be indexed based on a tetragonal cell ($P4/nmm$) of the ZrCuSiAs-type structure. According to the results of the Rietveld refinement[28] the impurity ThO_2 and SmAs phases in $Sm_{1-x}Th_xFeAsO$ [$x=0.00(2)$ and 0.08(3)] samples amount to less than ~10 at. % (Fig. 1). The amount of ThO_2 gradually increases with nominal Th content. It is important to notice that in the reported syntheses of Th-substituted GdFeAsO, NdFeAsO, LaFeAsO, $SmFeAsO_{1-y}F_y$, and TbFeAsO (Refs. 17–21) ThO_2 oxide was used as a source of Th, and the obtained samples always contained ThO_2 as an impurity. To minimize the appearance of this parasitic phase we used ThAs in the starting mixture but we were not able to suppress the formation of the ThO_2 phase. Thus, the nominal/initial compositions of the polycrystalline samples do not agree with the real composition, as we also quantify later in the structure analysis. Because the ionic radius of Th^{4+} ($r_{Th}^{ion} \sim 0.95$ Å) is smaller than that of Sm^{3+} ($r_{Sm}^{ion} \sim 1.04$ Å) (Ref. 31) one can expect the lattice to shrink as a result of the Th substitution. Indeed, compared to SmFeAsO [$a=3.9427(1)$ Å and $c=8.4923(3)$ Å], both lattice parameters changed to $a=3.9357(2)$ Å and $c=8.4327(5)$ Å for $x=0.10(5)$. Though the a axis changes only slightly, the c axis shortens significantly with Th substitution, indicating that Th is indeed incorporated into the lattice. A similar trend in the shrinkage of the c axis has been observed for the $Gd_{1-x}Th_xFeAsO$, $Nd_{1-x}Th_xFeAsO$, $La_{1-x}Th_xFeAsO$, and $Sm_{0.9}Th_{0.1}FeAsO_{1-y}F_y$ systems[17–20] and was attributed to

strengthening of the interlayer Coulomb attraction as a consequence of Th doping. In contrast to the above behavior, in the $Tb_{1-x}Th_xFeAsO$ system[21] both lattice parameters increase with increasing x since the ionic size of Th^{4+} is larger than that of Tb^{3+}.

The evolution of $Sm_{1-x}Th_xFeAsO$ crystal structure was studied using powder XRD for the samples with $x=0.00(2)$, 0.08(3), and 0.10(5). It is well known that the parent compound SmFeAsO crystallizes in a $P4/nmm$ tetragonal structure at high temperatures but undergoes a transformation to *Cmma* orthorhombic symmetry at low temperatures.[32] This transformation is accompanied by a spin-density-wave (SDW) formation, typical for the undoped *Ln*FeAsO systems.[33] However, upon substitution the SDW and structural transition are suppressed and superconductivity appears. Several investigations have addressed this issue but there is controversy if the orthorhombic distortion survives when the material becomes superconducting (see Ref. 34, and references therein). We addressed this question in the $Sm_{1-x}Th_xFeAsO$ system. Figure 2 shows low-temperature XRD patterns for three Th-substituted samples [$x=0.00(2)$, 0.08(3), and 0.10(5)]. By monitoring the gradual evolution of XRD patterns at low temperatures we paid special attention to the (220) peaks. No splitting or broadening of the (220) reflection was found down to liquid-helium temperature, indicating the absence of any structural transformation. Even for slightly Th-doped [$x=0.00(2)$] bulk superconducting sample, we were not able to resolve any definite inflection point in the evolution of full width at half maximum with temperature, which could be a sign of a structural transformation (see inset in the lower panel of Fig. 2). Therefore, our data support a picture of a rather abrupt suppression of the orthorhombic phase at the boundary to superconductivity, as observed, e.g., in $PrFeAsO_{1-x}F_x$.[35]

The refined structural data for polycrystalline samples of $Sm_{1-x}Th_xFeAsO$ are summarized in Table I. Since ThO_2 and SmAs were observed as impurity phases they were included in the refinement (using a multiphase Rietveld code). The Rietveld refinement of the structure using powder x-ray diffraction data for all temperatures between liquid-helium temperature and room temperature converged at $R_B=1.1-2.3$ %, $R_F=1.2-2.1$ % for $x=0.00(2)$; $R_B=1.8-2.9$ %, $R_F=1.7-2.4$ % for $x=0.08(3)$; $R_B=2.0-2.3$ %, $R_F=1.6-1.9$ % for $x=0.10(5)$; $R_p\sim 2.6\%$, $R_{wp}\sim 3.8\%$ (not corrected for background); and $R_p\sim 7.0\%$, $R_{wp}\sim 8.3\%$ (conventional Rietveld R factors).

Figure 3 shows the temperature dependence of the lattice parameters a and c, the unit-cell volume V, and the relative thermal expansion $\Delta a/a$ and $\Delta c/c$. The error bars are not always visible since the uncertainty in the determination of quantities is smaller than the size of the symbols. The coefficients of thermal expansion were calculated from the change in the unit-cell parameters, approximated by a linear temperature dependence, in the range between 200 and 300 K. The linear thermal-expansion coefficients α_a and α_c vary not much with Th content, however the thermal expansion is strongly anisotropic. At 295 K, α_c is about four times larger than α_a [$21.7(1.6)\times 10^{-6}$ K^{-1} and $6(1)\times 10^{-6}$ K^{-1}, respectively]. The thermal expansion along the c axis can be seen as a sum of the changes in the Fe_2As_2 layer, the $(Sm,Th)_2O_2$

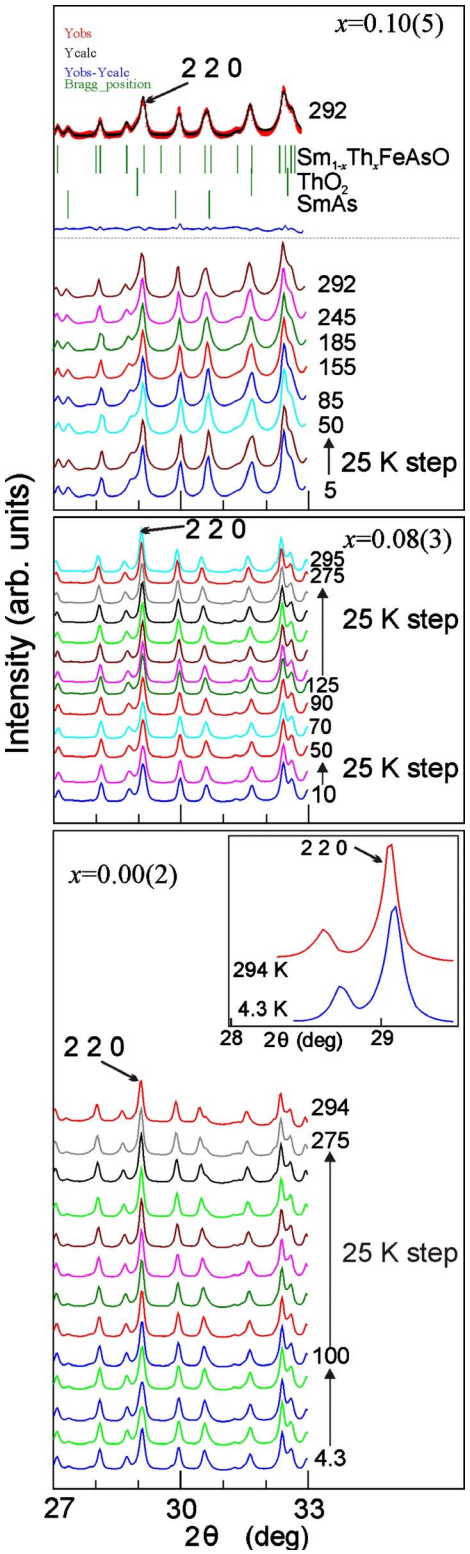

FIG. 2. (Color online) XRD patterns for $Sm_{1-x}Th_xFeAsO$ samples with $x=0.10(5)$, 0.08(3), and 0.00(2). On the top of upper panel the upper lines (red and black) represent the experimental data and calculated profile, the lower line (blue) is the difference curve, bars (green) mark the calculated position of the reflections for phases constituting the samples. Temperatures in kelvin are given on the right site. Inset in the lower panel shows the absence of broadening of the (220) reflections.

TABLE I. Refined structural parameters for $Sm_{1-x}Th_xFeAsO$ samples measured at 15 and 295 K. The lattice is tetragonal with space group $P4/nmm$.

Starting composition, T_c (K)	$Sm_{0.7}Th_{0.3}FeAsO$, 51.5		$Sm_{0.85}Th_{0.15}FeAsO$, 42		$Sm_{0.92}Th_{0.08}FeAsO$, 38	
Data collection T (K)	15	295	15	295	15	295
a (Å)	3.9357(2)	3.9404(2)	3.9381(3)	3.9433(3)	3.9391(2)	3.9427(1)
c (Å)	8.4327(5)	8.4730(6)	8.4475(3)	8.4810(6)	8.4540(4)	8.4885(3)
V (Å)	130.62(1)	131.56(1)	131.00(2)	131.87(2)	131.18(1)	131.955(8)
Sm/Th z	0.1424(3)	0.1421(3)	0.1393(2)	0.1389(2)	0.1387(2)	0.1385(2)
B_{iso} [a] (Å^2)	1.31(9)	1.6(1)	3.85(6)	3.54(6)	1.68(9)	2.06(7)
Occupation Sm/Th	0.88/0.12(4)	0.90/0.10(5)	0.92/0.08(3)	0.92/0.08(3)	1.00/0.00(2)	1.00/0.00(2)
Fe B_{iso} (Å^2)	1.3(2)	1.9(2)	3.9(1)	3.8(1)	2.2(2)	2.3(1)
z_{As}	0.6595(7)	0.6618(7)	0.6603(4)	0.6612(3)	0.6597(5)	0.6609(4)
B_{iso} (Å^2)	1.8(2)	2.4(2)	4.4(1)	4.1(1)	2.2(2)	2.6(1)
O B_{iso} (Å^2)	5.3(9)	3.6(9)	1.8(4)	1.8(4)	1.8(6)	1.1(5)
R_p (%)	2.51[b](6.91[c])	2.34(7.57)	2.06(7.49)	1.87(7.30)	1.66(7.31)	1.00(6.66)
R_{wp} (%)	3.77(8.27)	3.66(9.17)	2.68(6.91)	2.39(6.51)	2.31(7.12)	1.38(5.77)
Sm/Th-As (4×) (Å)	3.246(3)	3.244(3)	3.258(2)	3.263(2)	3.266(2)	3.267(2)
Sm-O (4×) (Å)	2.305(1)	2.309(1)	2.2937(8)	2.2969(7)	2.2918(9)	2.2955(9)
Fe-As (4×) (Å)	2.384(3)	2.400(3)	2.391(2)	2.399(1)	2.388(2)	2.398(2)
Fe-Fe (4×) (Å)	2.78299(2)	2.78632(2)	2.78469(2)	2.78830(2)	2.78539(1)	2.787932(8)
As_1-Fe-As_2, β (deg)	108.6(3)	109.0(3)	108.8(2)	108.9(1)	108.6(2)	108.9(2)
As_2-Fe-As_3, α (deg)	111.3(1)	110.3(1)	110.90(6)	110.52(5)	111.14(8)	110.60(7)
s_3 [d] (Å)	1.671(6)	1.662(6)	1.692(4)	1.697(3)	1.704(4)	1.702(4)
s_1 [d] (Å)	2.402(5)	2.408(5)	2.354(3)	2.356(3)	2.345(4)	2.351(3)
s_2 [d] (Å)	2.69(1)	2.74(1)	2.708(6)	2.731(6)	2.700(8)	2.732(6)
h_{Pn} [d] (Å)	1.345(6)	1.371(6)	1.354(3)	1.3654(3)	1.350(4)	1.366(3)

[a]Debye-Waller factor.
[b]Not corrected for background.
[c]Conventional Rietveld R factors.
[d]Figure 4(a).

layer, and their separation (Sm,Th)-As distance. Remarkably, it is an increase in the Fe_2As_2 layer thickness that dominates the expansion, while the changes in the other structural building blocks are smaller, being on the order of 1/5 of that one in Fe_2As_2, and they compensate each other, since the As-Sm/Th appears to contract as much as the O-Sm/Th expands upon warming from 5 to 295 K. The anisotropic behavior of the thermal expansion is less pronounced at lower temperatures (Fig. 3). Within the present accuracy, the cell parameters vary continuously across the superconducting transition.

To document the effect of Th substitution in more detail we carried out single-crystal x-ray diffraction studies. Crystals from various batches were free of impurities, twins or intergrowing crystals and show well-resolved reflection patterns, indicating high-quality perfection. The structural refinement parameters of SmFeAsO and $Sm_{1-x}Th_xFeAsO$ single crystals are summarized in Table II. Since superconductivity in compounds of the 1111 family can be induced by oxygen deficiency,[11] in the refinement process the oxygen occupancy (O_{occ}) was allowed to vary. The values for O_{occ} for $Sm_{1-x}Th_xFeAsO$ and SmFeAsO samples were 1.04(4) and 1.02(2), respectively. Thus, in the final stage of the refinement the O_{occ} parameter was fixed to unity. An additional evidence that superconductivity in the studied samples was caused by Th substitution and not by oxygen deficiency is the absence of a strong shrinkage of the lattice, contrary to the one observed for superconducting oxygen-deficient SmFeAsO. According to Yang *et al.*,[36] 15% oxygen deficiency in $SmFeAsO_{0.85}$ causes the unit cell to shrink by $\Delta V/V = -2.9\%$ while for the Th-substituted crystals we observed $\Delta V/V$ as low as -0.8%. From the refinement, the Th content for the batch with starting composition $Sm_{0.65}Th_{0.35}FeAsO$ is only about 11 at. %. As for polycrystalline samples, the values of both the a and c lattice parameters of the parent compound are significantly larger than those of Th substituted. For 11 at. % substitution the relative changes are as follows: $\Delta c/c \sim -0.49\%$ and $\Delta a/a \sim -0.15\%$. Lee *et al.*[37] pointed out that there is a relationship between T_c and the As-Fe-As bond angle of the $FeAs_4$ tetrahedron; T_c is maximal when the As-Fe-As bond angle is close to 109.47, corresponding to an ideal tetrahedron. Several groups studied it theoretically,[38] and later Mizuguchi *et al.*[39] suggested that the pnictogen height (h_{Pn}) is an important parameter controlling T_c and the nesting properties of Fermi surfaces. This geometrical parameter h_{Pn} measures the distance between a pnictogen atom and the Fe layer, given numerically by $(z_{Pn}-0.5)\times c$, where z_{Pn} is the internal coordinate of the pnictogen atom and c the

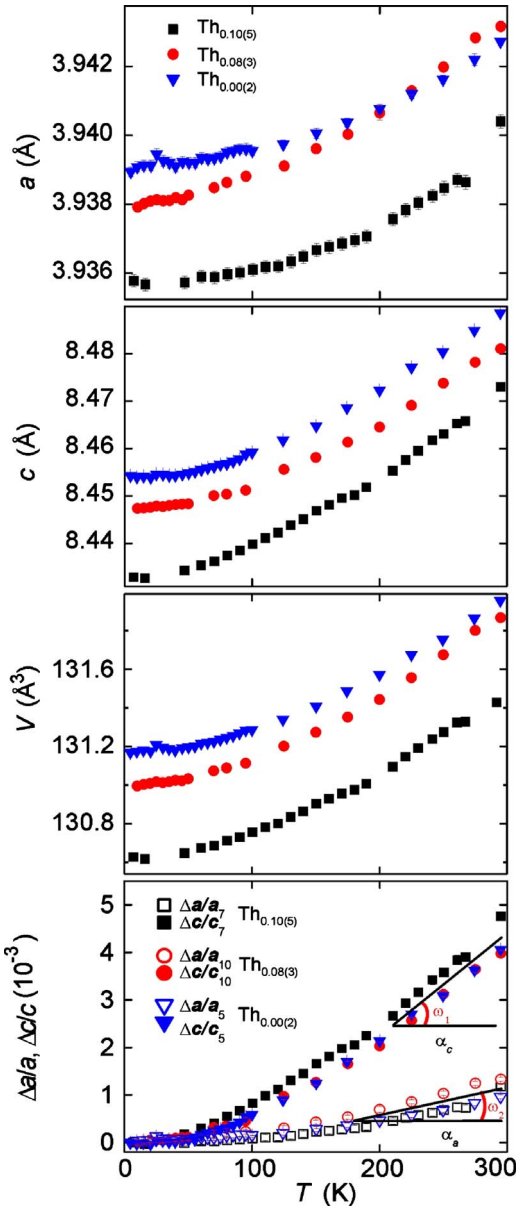

FIG. 3. (Color online) Temperature dependence of the structure parameters a and c, elementary cell volume V, and of the relative thermal expansions $\frac{\Delta a}{a_T}$, $\frac{\Delta c}{c_T}$ for the three $Sm_{1-x}Th_xFeAsO$ compositions. The thermal-expansion coefficients were calculated from the change in the unit-cell parameters, approximated by a linear temperature dependence, in the range between 200 and 300 K (tangent of the angles ω_1 and ω_2). The obtained values are equal to $\alpha_a = 6(1) \times 10^{-6}$ K^{-1} and $\alpha_c = 21.7(1.6) \times 10^{-6}$ K^{-1} for the expansion along the a and c axes, respectively.

c-axis lattice constant. As it was shown in Ref. 38, z_{Pn} controls the relative position of the $d_{x^2-y^2}(=d_{xy})$ and d_{z^2} bands near the Γ point of the Brillioun zone. All together these findings indicate that the superconducting properties of the Fe-based superconductors are correlated with the crystal structure. Our structure information obtained from single-crystal refinement shows that the As-Fe-As bond angles, α and β, are very close to those of a regular tetrahedron and they are almost independent of Th substitution. The value of $h_{Pn} \sim 1.37$ Å is very close to its optimal value and almost insensitive to Th substitution (see Tables I and II). Similar results were found for F-doped SmFeAsO single crystals.[40] Bearing all this in mind we conclude that intrinsically the geometry of $FeAs_4$ tetrahedron in SmFeAsO is close to optimal for having a high T_c and the geometry does not change significantly when we introduce charge carriers through heterovalent substitution in the Sm_2O_2 layer.

The effect of Th substitution is shown schematically in Fig. 4(a). With increasing Th content the main metric parameters vary systematically: both unit-cell parameters (a,c) shrink, the fractional atomic coordinate of the As site z_{As} remains almost unchanged, while that of Sm/Th $z_{Sm/Th}$ increases. The As-Sm/Th distance shortens and the O-Sm/Th distance elongates (Tables I and II). Equivalently one may focus on the "layers" of the structure: the Sm/ThO layer expands ($\Delta s_1 = 0.055$ Å), the AsFe layer remains unaffected, and the distance s_3 between the Sm/ThO and the AsFe layers shortens by $\Delta s_3 = -0.048$ Å (Table II). These changes can be rationalized by considering the degree of covalent and ionic bonding character,[40] and the fact that the ionic radius of tetravalent Th is smaller than that of trivalent Sm whereas Th has a larger covalent radius than that of Sm ($r_{Th}^{cov} \sim 1.65$ Å and $r_{Sm}^{cov} \sim 1.62$ Å). The same geometric changes in the unit cell due to Th doping were observed for polycrystalline samples (Table I). Thorium substitution has almost no effect on the geometry of the $FeAs_4$ tetrahedron, whereas it expands considerably along the c direction with increasing temperature [Fig. 4(b)]. The angle $\alpha(\beta)$ becomes smaller (larger) and h_{Pn} becomes larger for $Sm_{0.90(5)}Th_{0.10(5)}FeAsO$ in the temperature range between 15 and 295 K: $\Delta\alpha = -1°$, $\Delta\beta = 0.4°$, $\Delta h_{Pn} = 0.02$ Å. The pnictogen height as a function of temperature for three Th compositions is shown in Fig. 4(c). It varies in the same manner for all studied samples from ~1.37 Å at 295 K to ~1.35 Å at 5 K.

B. Magnetic properties

The temperature dependence of the magnetic susceptibility for polycrystalline samples of $Sm_{1-x}Th_xFeAsO$ in a magnetic field of 0.5 mT, measured after zero-field cooling (ZFC) is shown in Fig. 5. The superconducting volume fraction estimated at 5 K varies from 100% for $x = 0.10(5)$ to ~30% for $x = 0.00(2)$, which indicates on the bulk superconductivity of the studied compounds. The inhomogeneity of the Th distribution at low levels of doping $[x = 0.00(2)]$ leads to a broadening of the transition. With increasing Th content the superconducting transition become narrower and shift to higher temperatures and T_c reaches a maximum value of ~51.5 K for $x = 0.10(5)$.

Initial magnetization curves recorded for polycrystalline $Sm_{0.90(5)}Th_{0.10(5)}FeAsO$ in the temperature range between 2 and 40 K indicate that the intergranular lower critical field H_{c1}^* is very high (Fig. 6), indicative for good connections between grains. This is confirmed by results of minor hysteresis loops measurements, performed in the zero-field cooled mode, in the field range before flux is trapped within grains.[41] In the inset of Fig. 6 the intergrain critical current density is shown for polycrystalline $Sm_{0.90(5)}Th_{0.10(5)}FeAsO$ estimated in the temperature range from 2 to 40 K applying

TABLE II. Structure refinement parameters of SmFeAsO and $Sm_{1-x}Th_xFeAsO$ single crystals. The diffraction measurements were performed at 295(2) K using Mo $K\alpha$ radiation. The lattice is tetragonal, $P4/nmm$ space group with $Z=2$, atomic coordinates: Sm/Th on 2*c* (1/4, 1/4, z_{Sm}), Fe on 2*b* (3/4, 1/4, 1/2), As on 2*c* (1/4, 1/4, z_{As}), and O on 2*a* (3/4, 1/4, 0). The absorption correction was done analytically. A full-matrix least-squares method was employed to optimize F^2. Some distances and marking of atoms are shown in Fig. 4.

Empirical formula	SmFeAsO	$Sm_{0.89}Th_{0.11}FeAsO$, (T_c=49.5 K)
a (Å)	3.9427(1)	3.9369(1)
c (Å)	8.4923(3)	8.4510(6)
V (Å^3)	132.012(7)	30.984(10)
z_{Sm} (atomic coordinate)	0.1372(1)	0.1411(1)
B_{iso} [a] (Å^2)	0.79(8)	0.71(8)
Occupation Sm/Th	1.00(2)	0.89(2)/0.11(2)
z_{As}	0.6603(1)	0.6611(1)
B_{iso} (Å^2)	0.79(8)	0.79(8)
B_{iso}(O) (Å^2)	0.95(8)	0.63(8)
B_{iso}(Fe) (Å^2)	0.95(8)	0.87(8)
Sm_1-Sm_2 (Å)	3.6340(3)	3.6658(7)
Sm_2-Sm_3(a) (Å)	3.9427(1)	3.9369(1)
O-O=Fe-Fe (Å)	2.7879	2.7838
Sm_2-As_2 (Å)	3.2756(5)	3.2469(9)
Sm-O (Å)	2.2901(2)	2.3015(4)
As_2-As_3(a) (Å)	3.9427(1)	3.9369(1)
As_1-As_2 (Å)	3.8963(9)	3.8945(15)
Fe-As (Å)	2.3955(6)	2.3937(9)
As_1-Fe-As_2, β (deg)	108.83(2)	108.89(3)
As_2-Fe-As_3, α (deg)	110.76(4)	110.64(6)
s_3 [b] (Å)	1.720(1)	1.672(1)
s_1 [b] (Å)	2.330(2)	2.385(2)
s_2 [b] (Å)	2.723(2)	2.723(2)
h_{pn} [b] (Å)	1.3613(9)	1.3615(9)
Calculated density (g/cm^3)	7.475	7.761
Absorption coefficient (mm^{-1})	39.606	43.713
F(000)	258	264
Crystal size (μm^3)	137(2.5)×90(2.5)×18(2.5)	71(2.5)×67(2.5)×18(2.5)
Θ range for data collection (deg)	4.80–47.11	4.82–45.88
Index ranges	$-6\leqslant h\leqslant 8$, $-8\leqslant k\leqslant 7$, $-17\leqslant l\leqslant 17$	$-6\leqslant h\leqslant 7$, $-6\leqslant k\leqslant 7$, $-16\leqslant l\leqslant 13$
Reflections collected/unique	3106/399 R_{int}=0.0643	2229/376 R_{int}=0.0457
Completeness to 2Θ (%)	98.5	98.9
Data/restraints/parameters	399/0/11	376/0/12
Goodness of fit on F^2	1.057	1.080
Final R indices [$I>2\sigma(I)$]	R_1=0.0383, wR_2=0.0921	R_1=0.0454, wR_2=0.1030
R indices (all data)	R_1=0.0402, wR_2=0.0933	R_1=0.0591, wR_2=0.1049
$\Delta\rho_{max}$ and $\Delta\rho_{min}$ (e/Å^3)	9.459 and −5.773	12.052 and −3.329

[a]Debye-Waller factor.
[b]Figure 4(a).

Bean's model,[42] with the sample size in the plane perpendicular to the applied magnetic field direction. As shown in Fig. 7 the irreversibility line for polycrystalline $Sm_{0.90(5)}Th_{0.10(5)}FeAsO$ is well described by a power-law temperature dependence according to $(1-T/T_c)^n$ with a T_c =51.4(1) K and n=1.56(2) [straight line in the log-log H_{irr} vs $(1-T/T_c)$ dependence in the inset]. The value of n =1.56(2) is very close to n=3/2, the value predicted by Yeshurun and Malozemoff[43] for high-T_c superconductors characterized by small coherence length.

Magnetization measurements performed on a small lump sample mechanically extracted from the growth batch of nominal composition $Sm_{0.65}Th_{0.35}FeAsO$ show the highest onset T_c=53 K which is comparable to the maximum T_c reported for F doping.[2–4] Temperature and compositional gradients in the crucible may lead to variations in the Th

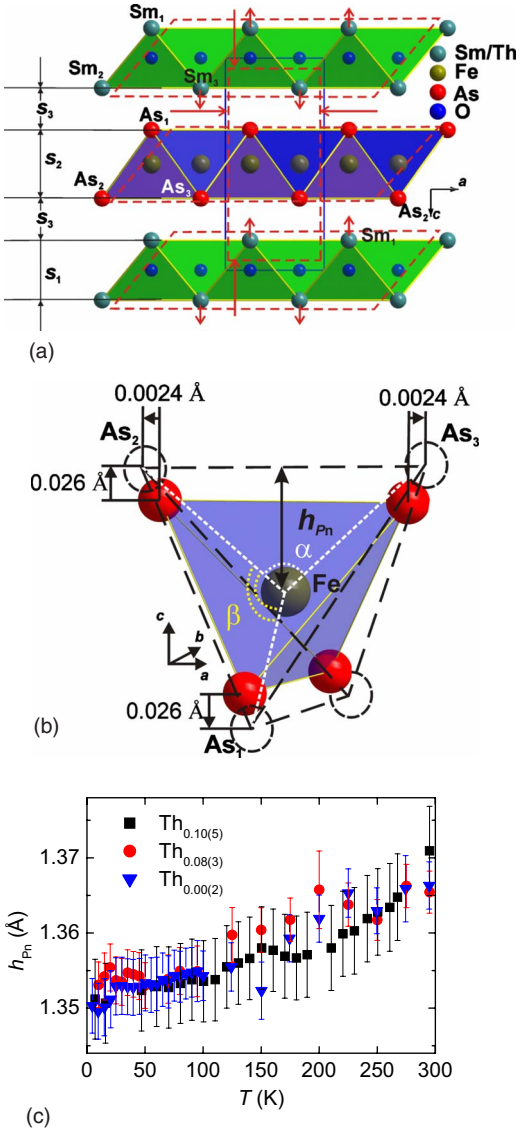

FIG. 4. (Color online) (a) Schematic representation of the projection of $Sm_{1-x}Th_xFeAsO$ lattice fragment on the *ac* plane and the changes in its dimensions (red dotted lines) with substitution of Sm by Th. (b) Schematic representation of the thermal expansion of $FeAs_4$ tetrahedron for $Sm_{0.90(5)}Th_{0.10(5)}FeAsO$ at 15 K (solid lines and circles) and 295 K (dotted lines and circles). (c) Pnictogen height (h_{Pn}) as a function of temperature for the three $Sm_{1-x}Th_xFeAsO$ compositions.

content of the crystals and differences in T_c, giving rise to a broad overall onset of diamagnetism. The temperature dependence of the magnetic moment measured in a magnetic field parallel to the *c* axis of a plate-like single crystal with mass of 100 ng and a composition of $Sm_{0.89(2)}Th_{0.11(2)}FeAsO$ is shown in Fig. 8. A sharp transition to the superconducting state with $T_{c,\mathrm{eff}}$=49.5 K is observed.

The anisotropic superconducting properties of single-crystalline samples were studied by analyzing the magnetic torque $\tau(\theta)=\mu_0 mH\sin(\theta)$, where θ denotes the angle between the applied magnetic field and the *c* axis of the crystal, μ_0 is the magnetic constant, *m*—the angular-dependent magnetic moment of a sample, and *H*—a magnitude of the applied magnetic field. Measurements of the magnetic torque, similar to those carried out on fluorine substituted SmFeAsO single crystals[30,44] were performed in order to investigate the anisotropic superconducting behavior in terms of the anisotropy parameter γ. The torque data were analyzed using a theoretical expression derived by Kogan *et al.*[45] within the London limit of the anisotropic Ginzburg-Landau theory,

$$\tau(\theta) = -\frac{V\Phi_0 H}{16\pi\lambda_{ab}^2}\left(1-\frac{1}{\gamma^2}\right)\frac{\sin(2\theta)}{\varepsilon(\theta)}\ln\left[\frac{\eta H_{c2}^{c}}{\varepsilon(\theta)H}\right] + A\sin(2\theta). \quad (1)$$

Here *V* is the crystal volume, Φ_0 is the elementary flux quantum, $H_{c2}^{\|c}$ is the upper critical field along the *c* axis, η denotes a numerical parameter on the order of unity, and $\varepsilon(\theta)=[\cos^2(\theta)+\gamma^{-2}\sin^2(\theta)]^{1/2}$. Demagnetization effects do not need to be taken into account in studies within the vortex state. Here, the internal and the external magnetic field of a superconductor are almost equal to each other since its magnetization is much smaller than the applied magnetic field strength. Accordingly, Eq. (1) is well suited to study anisotropic properties of a superconductor in the mixed state, as no assumptions on the shape of the sample needs to be in-

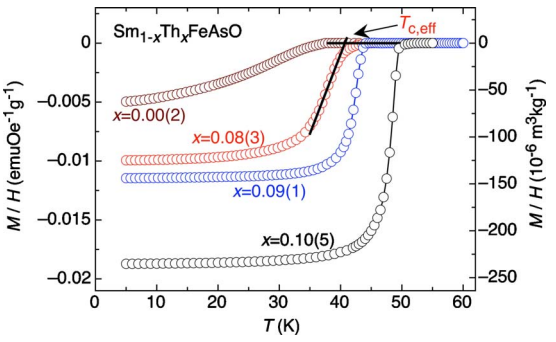

FIG. 5. (Color online) Temperature dependence of the magnetic susceptibility for $Sm_{1-x}Th_xFeAsO$ samples measured at 0.5 mT, after cooling in zero field. The determination of $T_{c,\mathrm{eff}}$ is illustrated. The values of *x* were determined on a basis of XRD refinement.

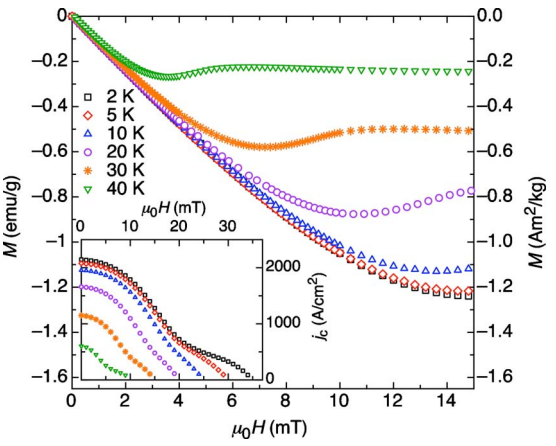

FIG. 6. (Color online) Field dependence of the initial magnetization for polycrystalline $Sm_{0.90(5)}Th_{0.10(5)}FeAsO$. Inset: field dependence of the intergrain critical current at various temperatures.

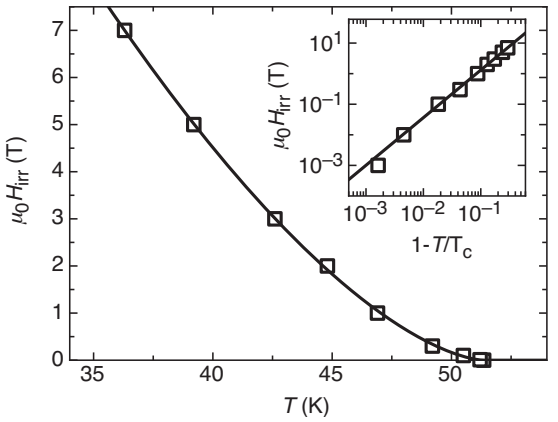

FIG. 7. Temperature dependence of the irreversibility field H_{irr} for polycrystalline $Sm_{0.90(5)}Th_{0.10(5)}FeAsO$. The irreversibility line is approximated well by a power-law temperature dependence with an exponent $n \approx 3/2$ (solid line), as discussed in the text. The inset presents the log-log H_{irr} vs $(1-T/T_c)$ dependence.

cluded. The needed volume V in Eq. (1) of the crystal used here, which quality was presented in Fig. 8 already, is difficult to determine accurately due to its very small mass of approximately 100 ng. We estimated V by measurements of the magnetic moment using a superconducting quantum interference device magnetometer at low magnetic fields where the Meissner state is entered. Note that for analyzing the anisotropy parameter γ by Eq. (1), the error in estimating the crystals volume is negligible, since γ has direct influence of the angular dependence of the torque. Representative example of angular-dependent torque curves measured at 45 K in a magnetic field of 1.2 T is shown in Fig. 9. The presence of a finite torque as well as a strongly angular-dependent irreversibility clearly reveals the pronounced anisotropy of the superconducting state. A pronounced irreversibility close to the *ab* plane (90°) is observed, associated with a very high vortex pinning in this field direction with respect to the crystallographic orientation. The peak-like feature very close to 90° is likely related with a lock-in effect of vortices within the *ab* plane, where for fields close to the in-plane orientation, vortices tend to align spontaneously strictly along to the

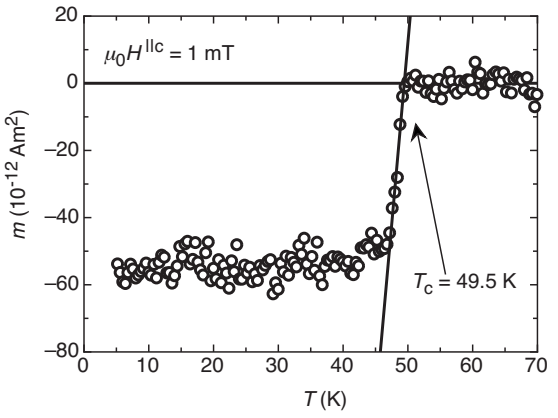

FIG. 8. Temperature dependence of the magnetic moment for a single crystal of $Sm_{0.89(2)}Th_{0.11(2)}FeAsO$ measured in ZFC mode in a magnetic field of 1 mT applied parallel to the *c* axis.

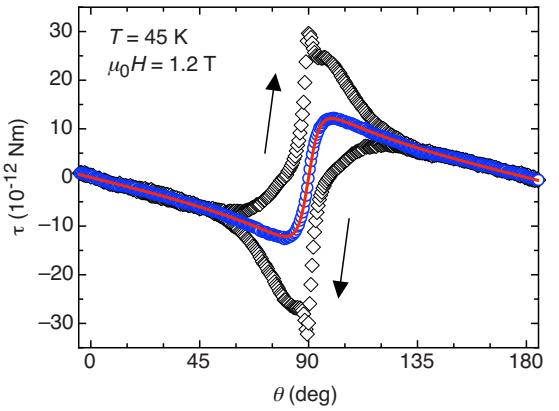

FIG. 9. (Color online) Angular dependence of the raw (diamonds) and the reversible (circles) torque data of a $Sm_{0.89(2)}Th_{0.11(2)}FeAsO$ single crystal at T=45 K and in a magnetic field of 1.2 T. Clear indications of a lock-in effect of vortices are observed close to the *ab* plane. The solid curve represents a fit of $\tau(\theta)$, given in Eq. (1), to the reversible torque data (circles).

ab plane,[46] indicative of high crystal perfection. If imperfection or impurity pinning effects dominate, the lock-in effect cannot be resolved, usually ascribed to intrinsic pinning of vortices due to the anisotropic crystal structure.

Note that the anisotropy parameter γ derived from the present analysis in rather low magnetic fields equals the magnetic penetration depth anisotropy γ_λ.[30] The derived results of $\gamma_\lambda(T)$ are shown in Fig. 10, γ_λ increase from ~9.8 at 47 K to ~13.2 at 38 K. Unfortunately, due to the pronounced vortex pinning in this crystal, especially close to the *ab* plane, torque data below 38 K could not be reliably analyzed. The observed temperature dependence of γ_λ is in good agreement with $\gamma_\lambda(T)$ found for fluorine substituted SmFeAsO and NdFeAsO.[30,44] Obviously, the $Sm_{1-x}Th_xFeAsO$, $SmFeAsO_{1-x}F_y$, and $NdFeAsO_{1-x}F_y$ are much more anisotropic superconductors than, e.g., doped $BaFe_2As_2$, doped $SrFe_2As_2$, and $FeSe_{0.5}Te_{0.5}$, with $\gamma_\lambda \sim 2-3$.[47–52] This is most probably related to the more pronounced "layering" of the crystal structure in the 1111 systems, as compared to other known iron-based superconductors.

Magnetization hysteresis loops of a relatively large single crystal of $Sm_{1-x}Th_xFeAsO$ (~500 ng) measured at various

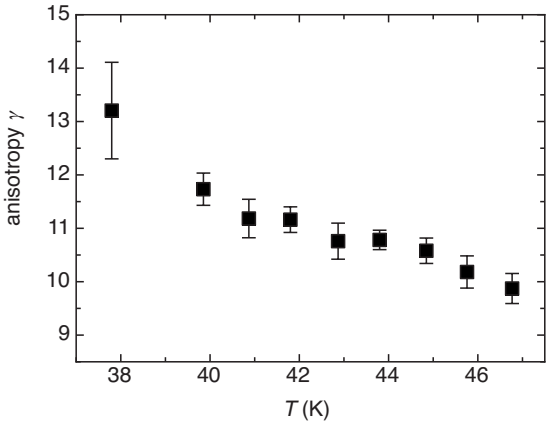

FIG. 10. Temperature dependence of the anisotropy parameter γ_λ obtained from the fits of torque data (e.g., Fig. 9).

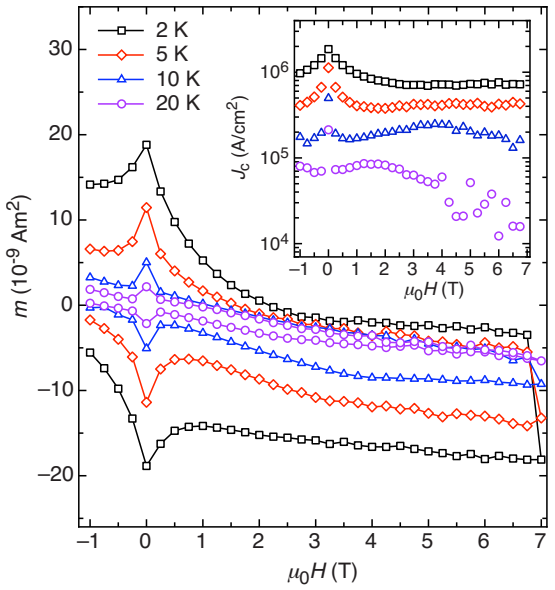

FIG. 11. (Color online) Magnetic hysteresis loops measured on a single crystal at 2, 5, 10, and 20 K in a field up to 7 T parallel to the c axis. Inset: critical current density calculated from the width of the hysteresis loops.

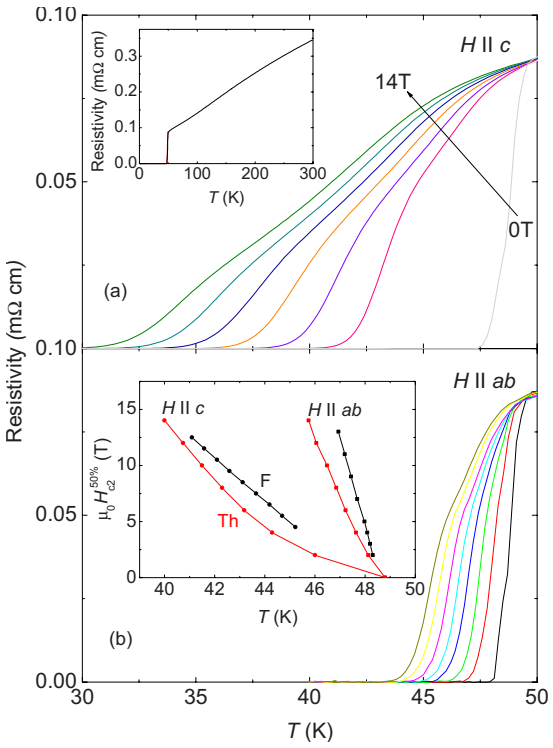

FIG. 12. (Color online) Temperature dependences of the resistivity for a $Sm_{0.89(2)}Th_{0.11(2)}FeAsO$ single crystal measured with the field applied (a) parallel to Fe_2As_2 layers ($H\|ab$) and (b) perpendicular to them ($H\|c$), in various magnetic fields (0, 2, 4, 6, 8, 10, 12, and 14 T). Inset of (a) shows the resistivity in the temperature range of 2–300 K. Inset of (b) shows temperature dependence of the upper critical field with $H\|ab$ and $H\|c$. To determine H_{c2} the 50% ρ_n criterion was used. The data for $SmFeAsO_{0.7}F_{0.25}$ (nominal composition) crystal were taken from Ref. 40.

temperatures below T_c in magnetic fields up to 7 T applied parallel to the crystal c axis are presented in Fig. 11. The wide loops, with a width almost independent of the field, indicate a rather high critical current density (J_c) in the sample. The J_c estimated from the width of the hysteresis loop using Bean's model is at 2 K close to 10^6 A cm^{-2} in the field range investigated (see the inset in Fig. 11). The slight increase in critical current density for higher magnetic fields may indicate an increase in the effectiveness of pinning centers giving rise to a "peak effect." A similar behavior was found in F-doped SmFeAsO single crystals.[22,23,40]

C. Magnetoresistance

The inset to the upper panel of Fig. 12 shows a typical cooldown resistivity curve. The resistivity in zero field decreases by a factor of 3.7 from room temperature upon cooling to T_c (onset—49.7 K; 50%—48.9 K; zero—47.4 K), defining the so-called resistivity ratio of the sample studied here. Similar resistivity ratios are typically observed in SmFeAsO with various substitutions on the Fe, As, or O sites.[22,40,53] A very slight change in the slope near 125 K is observed, possibly due to phonon scattering or crystalline electric field effects. The magnetoresistance in fixed fields was recorded upon decreasing temperature starting from above T_c, to account for irreversibility effects (Fig. 12). From this data, the upper critical field was estimated, defined as the magnetic field, where 50% of the resistivity is suppressed of ρ_n (see inset in lower panel of Fig. 12), where ρ_n is the linear extrapolation of the normal state resistivity. In $Sm_{1-x}Th_xFeAsO$ magnetic fields cause only a slight shift of the onset of superconductivity, but a significant broadening of the transition, indicating weaker pinning and accordingly larger flux flow dissipation. Furthermore, two distinct slopes are visible in the temperature dependence of the resistivity recorded in magnetic field. This difference is not visible in zero magnetic field and thus two different transitions may be excluded. Such behavior has been widely observed in the 1111 family.[11,40] Interestingly, a similar broadening resistive transitions and developments of two distinct slopes with $H\|c$ was also observed in cuprate superconductors[54] and was interpreted in terms of a vortex-liquid state.[55,56] A recent report on $NdFeAsO_{1-x}F_x$ single crystals confirmed the existence of a vortex-liquid state in the 1111 system.[57] The upper critical field anisotropy γ_H, defined as a ratio of the upper critical field parallel to the ab plane, $H_{c2}^{\|ab}$, to the upper critical field parallel to the c axis, $H_{c2}^{\|c}$, is temperature dependent. The γ_H value at 46 K calculated with the upper critical field determined by the 50% of the resistivity criterion is about 6.4 and is smaller than the γ_λ value of about 9.8 at 47 K. This is in agreement with a tendency of increasing penetration depth anisotropy γ_λ and decreasing upper critical field anisotropy with decreasing temperature[40,58] since both anisotropies should converge at T_c.[30] The upper critical field slopes $\mu_0 dH_{c2}/dT \sim 5.4$ T/K for $H\|ab$ and ~ 2.7 T/K for $H\|c$ were determined using a linear part of $H_{c2}(T)$. These slopes suggest very high values of $H_{c2}(0)$. The ratio $dH_{c2}/dT_{(H\|ab)}/dH_{c2}/dT_{(H\|c)}$ provides a rough estimation of the upper critical field anisotropy γ_H for the temperatures

significantly below T_c leading, for the slopes values determined here, to a value of $\gamma_H(T=0)\approx 2$. These results confirm a tendency of decreasing γ_H with decreasing temperature, as already obtained from high-field resistivity measurements for $NdFeAsO_{1-x}F_x$ (Ref. 58) and $SmFeAsO_{1-x}F_y$.[40] Such a small value of the ratio $dH_{c2}/dT_{(H\|ab)}/dH_{c2}/dT_{(H\|c)}$ is mostly due to the enormous sensitivity of the steep $dH_{c2}/dT_{(H\|ab)}$ on Th doping. Although very similar in shape, its value is ~5.4 T/K in $Sm_{1-x}Th_xFeAsO$ and ~8 T/K in $SmFeAsO_{1-x}F_y$.[40] Furthermore, H_{c2} for $H\|c$ is steeper in $Sm_{1-x}Th_xFeAsO$.

IV. CONCLUSIONS

Polycrystalline and single-crystalline samples of $Sm_{1-x}Th_xFeAsO$ superconductors were successfully prepared using the high-pressure cubic anvil technique. Partial substitution of Sm^{3+} by Th^{4+} results in a decrease in the unit-cell volume and the appearance of bulk superconductivity with onset T_c higher than 50 K. Upon warming from 5 to 295 K the overall unit cell expands significantly more perpendicular to the layers than parallel to them. Remarkably, it is the increase in the Fe_2As_2-layer thickness that dominates the expansion, while the changes in the other layers are smaller and even compensate each other, since the As-Sm/Th distance appears to contract by about the same amount as the O-Sm/Th distance expands. Magnetic measurements performed on a crystal with a T_c=49.5 K show a relatively high critical current density of 10^6 A/cm^2 at 2 K almost independent of the magnetic field. The magnetic penetration depth anisotropy γ_λ increases with decreasing temperature. The upper critical fields H_{c2} in $Sm_{1-x}Th_xFeAsO$ extracted from the resistivity measurements is anisotropic with slopes of ~5.4 T/K ($H\|ab$ plane) and ~2.7 T/K ($H\|c$ axis), sufficiently far below T_c. The upper critical field anisotropy γ_H (very roughly estimated for the temperatures far below T_c) is in the range of ~2, consistent with the tendency of γ_H to decrease with decreasing temperature, as already reported for other $NdFeAsO_{1-x}F_x$ and $SmFeAsO_{1-x}F_y$ compounds. All together, the unusual temperature behavior of both anisotropy parameters, γ_λ and γ_H, observed in Th-substituted SmFeAsO further support a common multigap scenario proposed for FeAs-based superconductors.[30,40,44,59]

ACKNOWLEDGMENTS

We thank D. Chernyshov and Y. Filinchuk for their assistance at the Swiss-Norwegian Beamlines, ESFR, Grenoble, France. We also thank W. Steuer (ETH) for the use of the x-ray single-crystal diffractometer and D. C. Johnston (Ames Laboratory) for useful comments. This work was supported by the Swiss National Science Foundation through the National Center of Competence in Research MaNEP (Materials with Novel Electronic Properties), Project No. 124616 and the Polish Ministry of Science and Higher Education, within the research project for the years 2007-2010 (Grant No. N N202 4132 33).

*zhigadlo@phys.ethz.ch

[1] Y. Kamihara, T. Watanabe, M. Hirano, and H. Hosono, J. Am. Chem. Soc. **130**, 3296 (2008).
[2] X. H. Chen, T. Wu, G. Wu, R. H. Liu, H. Chen, and D. F. Fang, Nature (London) **453**, 761 (2008).
[3] G. F. Chen, Z. Li, D. Wu, G. Li, W. Z. Hu, J. Dong, P. Zheng, J. L. Luo, and N. L. Wang, Phys. Rev. Lett. **100**, 247002 (2008).
[4] Z.-A. Ren, J. Yang, W. Lu, W. Yi, X.-L. Shen, Z.-C. Li, G.-C. Che, X.-L. Dong, L.-L. Sun, F. Zhou, and Z.-X. Zhao, EPL **82**, 57002 (2008).
[5] Z.-A. Ren, G.-C. Che, X.-L. Dong, J. Yang, W. Lu, W. Yi, X.-L. Shen, Z.-C. Li, L.-L. Sun, F. Zhou, and Z.-X. Zhao, EPL **83**, 17002 (2008).
[6] P. Cheng, L. Fang, H. Yang, X.-Y. Zhu, G. Mu, H.-Q. Luo, Z.-S. Wang, and H.-H. Wen, Sci. China, Ser. G **51**, 719 (2008).
[7] Z.-A. Ren, J. Yang, W. Lu, W. Yi, G.-C. Che, X.-L. Dong, L.-L. Sun, and Z.-X. Zhao, Mater. Res. Innovations **12**, 105 (2008).
[8] J.-W. G. Bos, G. B. S. Penny, J. A. Rodgers, D. A. Sokolov, A. D. Huxley, and J. P. Attfield, Chem. Commun. (Cambridge) **2008**, 3634.
[9] Y. G. Shi, S. Yu, A. A. Belik, Y. Matsushita, M. Tanaka, Y. Katsuya, K. Kobayashi, Y. Hata, H. Yasuoka, K. Yamaura, and E. Takayama-Muromachi, Phys. Rev. B **80**, 104501 (2009).
[10] J. Yang, X.-L. Shen, W. Lu, W. Yi, Z.-C. Li, Z.-A. Ren, G.-C. Che, X.-L. Dong, L.-L. Sun, F. Zhou, and Z.-X. Zhao, New J. Phys. **11**, 025005 (2009).
[11] P. M. Shirage, K. Miyazawa, M. Ishikado, K. Kihou, C. H. Lee, N. Takeshita, H. Matsuhata, R. Kumai, Y. Tomioka, T. Ito, H. Kito, H. Eisaki, S. Shamoto, and A. Iyo, Physica C **469**, 355 (2009).
[12] A. S. Sefat, R. Jin, M. A. McGuire, B. C. Sales, D. J. Singh, and D. Mandrus, Phys. Rev. Lett. **101**, 117004 (2008); A. S. Sefat, A. Huq, M. A. McGuire, R. Jin, B. C. Sales, D. Mandrus, L. M. D. Cranswick, P. W. Stephens, and K. H. Stone, Phys. Rev. B **78**, 104505 (2008); P. C. Canfield, S. L. Bud'ko, N. Ni, J. Q. Yan, and A. Kracher, *ibid.* **80**, 060501(R) (2009); C. Wang, Y. K. Li, Z. W. Zhu, S. Jiang, X. Lin, Y. K. Luo, S. Chi, L. J. Li, Z. Ren, M. He, H. Chen, Y. T. Wang, Q. Tao, G. H. Cao, and Z. A. Xu, *ibid.* **79**, 054521 (2009); S. K. Kim, M. E. Tillman, H. Kim, A. Kracher, S. L. Bud'ko, R. Prozorov, and P. C. Canfield, Supercond. Sci. Technol. **23**, 054008 (2010).
[13] G. Cao, S. Jiang, X. Lin, C. Wang, Y. Li, Z. Ren, Q. Tao, C. Feng, J. Dai, Z. Xu, and F.-C. Zhang, Phys. Rev. B **79**, 174505 (2009).
[14] H. Wadati, I. Elfimov, and G. A. Sawatzky, arXiv:1003.2663v3 (unpublished).
[15] C. Wang, S. Jiang, Q. Tao, Z. Ren, Y. Li, L.-J. Li, C.-M. Feng, J.-H. Dai, G.-H. Cao, and Z.-A. Xu, EPL **86**, 47002 (2009).
[16] H.-H. Wen, G. Mu, L. Fang, H. Yang, and X.-Y.Zhu, EPL **82**, 17009 (2008).
[17] C. Wang, L.-J. Li, S. Chi, Z.–W. Zhu, Z. Ren, Y.-K. Li, Y.-T. Wang, X. Lin, Y.-K. Luo, S.-A. Jiang, X.-F. Xu, G.-H. Cao, and Z.-A. Xu, EPL **83**, 67006 (2008).
[18] M. Xu, F. Chen, C. He, H.-W. Ou, J.-F. Zhao, and D.-L. Feng, Chem. Mater. **20**, 7201 (2008).
[19] J. Prakash, S. J. Singh, S. Patnaik, and A. K. Ganguli, J. Phys.:

Condens. Matter **21**, 175705 (2009).
[20] Y.-K. Li, X. Lin, Q. Tao, H. Chen, C. Wang, L.-J. Li, Y.-K. Luo, M. He, Z.-W. Zhu, G.-H. Cao, and Z.-A. Xu, Chin. Phys. Lett. **26**, 017402 (2009).
[21] L.-J. Li, Y.-K. Li, Z. Ren, Y.-K. Luo, X. Lin, M. He, Q. Tao, Z.-W. Zhu, G.-H. Cao, and Z.-A. Xu, Phys. Rev. B **78**, 132506 (2008).
[22] P. J. W. Moll, R. Puzniak, F. Balakirev, K. Rogacki, J. Karpinski, N. D. Zhigadlo, and B. Batlogg, Nature Mater. **9**, 628 (2010).
[23] N. D. Zhigadlo, S. Katrych, Z. Bukowski, S. Weyeneth, R. Puzniak, and J. Karpinski, J. Phys.: Condens. Matter **20**, 342202 (2008).
[24] A. P. Hammersley, S. O. Svensson, M. Hanfland, A. N. Fitch, and D. Häusermann, High Press. Res. **14**, 235 (1996).
[25] J. Rodríguez-Carvajal, Physica B **192**, 55 (1993).
[26] Oxford Diffraction Ltd. XCALIBUR, CRYSALIS software system, version 1.171.32.15, 2008.
[27] G. Sheldrick, *SHELXS-97: Program for the Solution of Crystal Structures* (University of Göttingen, Germany, 1997).
[28] G. Sheldrick, *SHELXL-97: Program for the Refinement of Crystal Structures* (University of Göttingen, Germany, 1997).
[29] S. Kohout, J. Roos, and H. Keller, Rev. Sci. Instrum. **78**, 013903 (2007).
[30] S. Weyeneth, R. Puzniak, N. D. Zhigadlo, S. Katrych, Z. Bukowski, J. Karpinski, and H. Keller, J. Supercond. Novel Magn. **22**, 347 (2009).
[31] R. D. Shannon, Acta Crystallogr., Sect. A: Cryst. Phys., Diffr., Theor. Gen. Crystallogr. **32**, 751 (1976).
[32] S. Margadonna, Y. Takabayashi, M. T. McDonald, M. Brunelli, G. Wu, R. H. Liu, X. H. Chen, and K. Prassides, Phys. Rev. B **79**, 014503 (2009).
[33] D. C. Johnston, arXiv:1005.4392v2 (unpublished).
[34] Y. Kamihara, T. Nomura, M. Hirano, J. E. Kim, K. Kato, M. Takata, Y. Kobayashi, S. Kitao, S. Higashitaniguchi, Y. Yoda, M. Seto, and H. Hosono, New J. Phys. **12**, 033005 (2010).
[35] D. G. Gheorghe, R. J. Wijngaarden, C. Bell, and J. Aarts, Phys. Rev. B **80**, 144518 (2009).
[36] J. Yang, Z.-A. Ren, G.-C. Che, W. Lu, X.-L. Shen, Z.-C. Li, W. Yi, X.-L. Dong, L.-L. Sun, F. Zhou, and Z.-X. Zhao, Supercond. Sci. Technol. **22**, 025004 (2009).
[37] C.-H. Lee, A. Iyo, H. Eisaki, H. Kito, M. T. Fernandez-Diaz, T. Ito, K. Kihou, H. Matsuhata, M. Braden, and K. Yamada, J. Phys. Soc. Jpn. **77**, 083704 (2008).
[38] D. J. Singh and M.-H. Du, Phys. Rev. Lett. **100**, 237003 (2008); V. Vildosola, L. Pourovskii, R. Arita, S. Biermann, and A. Georges, Phys. Rev. B **78**, 064518 (2008); S. Lebègue, Z. P. Yin, and W. E. Pickett, New J. Phys. **11**, 025004 (2009); K. Kuroki, H. Usui, S. Onari, R. Arita, and H. Aoki, Phys. Rev. B **79**, 224511 (2009).
[39] Y. Mizuguchi, Y. Hara, K. Deguchi, S. Tsuda, T. Yamaguchi, K. Takeda, H. Kotegawa, H. Tou, and Y. Takano, Supercond. Sci. Technol. **23**, 054013 (2010).
[40] J. Karpinski, N. D. Zhigadlo, S. Katrych, Z. Bukowski, P. Moll, S. Weyeneth, H. Keller, R. Puzniak, M. Tortello, D. Daghero, R. Gonnelli, I. Maggio-Aprile, Y. Fasano, Ø. Fischer, K. Rogacki, and B. Batlogg, Physica C **469**, 370 (2009).
[41] R. Puźniak, D.-X. Chen, E. M. Gyorgy, and K. V. Rao, J. Appl. Phys. **65**, 4344 (1989).
[42] C. P. Bean, Phys. Rev. Lett. **8**, 250 (1962); Rev. Mod. Phys. **36**, 31 (1964).
[43] Y. Yeshurun and A. P. Malozemoff, Phys. Rev. Lett. **60**, 2202 (1988).
[44] S. Weyeneth, R. Puzniak, U. Mosele, N. D. Zhigadlo, S. Katrych, Z. Bukowski, J. Karpinski, S. Kohout, J. Roos, and H. Keller, J. Supercond. Novel Magn. **22**, 325 (2009).
[45] V. G. Kogan, Phys. Rev. B **24**, 1572 (1981).
[46] S. Kohout, T. Schneider, J. Roos, H. Keller, T. Sasagawa, and H. Takagi, Phys. Rev. B **76**, 064513 (2007).
[47] Z. Bukowski, S. Weyeneth, R. Puzniak, P. Moll, S. Katrych, N. D. Zhigadlo, J. Karpinski, H. Keller, and B. Batlogg, Phys. Rev. B **79**, 104521 (2009).
[48] N. Ni, S. L. Bud'ko, A. Kreyssig, S. Nandi, G. E. Rustan, A. I. Goldman, S. Gupta, J. D. Corbett, A. Kracher, and P. C. Canfield, Phys. Rev. B **78**, 014507 (2008).
[49] H. Q. Yuan, J. Singleton, F. F. Balakirev, S. A. Baily, G. F. Chen, J. L. Luo, and N. L. Wang, Nature (London) **457**, 565 (2009).
[50] G. F. Chen, Z. Li, J. Dong, G. Li, W. Z. Hu, X. D. Zhang, X. H. Song, P. Zheng, N. L. Wang, and J. L. Luo, Phys. Rev. B **78**, 224512 (2008).
[51] Y. J. Jo, J. Jaroszynski, A. Yamamoto, A. Gurevich, S. C. Riggs, G. S. Boebinger, D. Larbalestier, H. H. Wen, N. D. Zhigadlo, S. Katrych, Z. Bukowski, J. Karpinski, R. H. Liu, H. Chen, X. H. Chen, and L. Balicas, Physica C **469**, 566 (2009).
[52] M. Bendele, S. Weyeneth, R. Puzniak, A. Maisuradze, E. Pomjakushina, K. Conder, V. Pomjakushin, H. Luetkens, S. Katrych, A. Wisniewski, R. Khasanov, and H. Keller, Phys. Rev. B **81**, 224520 (2010).
[53] Y. Kamihara, H. Hiramatsu, M. Hirano, Y. Kobayashi, S. Kitao, S. Higashitaniguchi, Y. Yoda, M. Seto, and H. Hosono, Phys. Rev. B **78**, 184512 (2008).
[54] W. K. Kwok, S. Fleshler, U. Welp, V. M. Vinokur, J. Downey, G. W. Crabtree, and M. M. Miller, Phys. Rev. Lett. **69**, 3370 (1992); W. K. Kwok, J. Fendrich, S. Fleshler, U. Welp, J. Downey, and G. W. Crabtree, *ibid.* **72**, 1092 (1994); H. Safar, P. L. Gammel, D. A. Huse, D. J. Bishop, J. P. Rice, and D. M. Ginsberg, *ibid.* **69**, 824 (1992).
[55] S. L. Lee, P. Zimmermann, H. Keller, M. Warden, I. M. Savić, R. Schauwecker, D. Zech, R. Cubitt, E. M. Forgan, P. H. Kes, T. W. Li, A. A. Menovsky, and Z. Tarnawski, Phys. Rev. Lett. **71**, 3862 (1993).
[56] G. Blatter, M. V. Feigel'man, V. B. Geshkenbein, A. I. Larkin, and V. M. Vinokur, Rev. Mod. Phys. **66**, 1125 (1994).
[57] Z. Pribulova, T. Klein, J. Kacmarcik, C. Marcenat, M. Konczykowski, S. L. Bud'ko, M. Tillman, and P. C. Canfield, Phys. Rev. B **79**, 020508(R) (2009).
[58] J. Jaroszynski, F. Hunte, L. Balicas, Y.-J. Jo, I. Raičević, A. Gurevich, D. C. Larbalestier, F. F. Balakirev, L. Fang, P. Cheng, Y. Jia, and H. H. Wen, Phys. Rev. B **78**, 174523 (2008).
[59] R. S. Gonnelli, D. Daghero, M. Tortello, G. A. Ummarino, V. A. Stepanov, R. K. Kremer, J. S. Kim, N. D. Zhigadlo, and J. Karpinski, Physica C **469**, 512 (2009); D. Daghero, M. Tortello, R. S. Gonnelli, V. A. Stepanov, N. D. Zhigadlo, and J. Karpinski, Phys. Rev. B **80**, 060502(R) (2009); J. Supercond. Novel Magn. **22**, 543 (2009); L. Malone, J. D. Fletcher, A. Serafin, A. Carrington, N. D. Zhigadlo, Z. Bukowski, S. Katrych, and J. Karpinski, Phys. Rev. B **79**, 140501(R) (2009).